Proceedings of the 2003 IEEE/RSJ
Intl. Conference on Intelligent Robots and Systems
Las Vegas, Nevada · October 2003

Contact Sensing for Parts Localization: Sensor Design and Experiments*

Yan-Bin Jia

Department of Computer Science
Iowa State University
Ames, IA 50011-1040, U.S.A.
jia@cs.iastate.edu

Abstract

A 2-axis force/torque sensor has been designed for contact sensing and the localization of 2-D curved shapes. The sensor is an aluminum piece attached with two "chip sensors", each a half-bridge circuit consisting of two strain gauges. It functions like a "wrist" which uses the two chip sensors to detect bending and twisting moments, respectively. When an external force is exerted on a jaw mounted with the F/T sensor, the point of force application is linearly related to the ratio between the reading variations from the chip sensors. This principle is used for determining contact locations on the jaw after calibration. A simple strategy is later described to control the jaw to roll on a motionless 2-D object while estimating the movement of contact. Given its shape, the object's position and orientation relative to the jaw can also be estimated during the rolling motion. Experiments have been conducted with an Adept Cobra 600 manipulator.

1 Introduction

Force/torque and tactile sensors have been used in a wide range of tasks from shape perception and recognition to grasping and dexterous manipulation. They play an important role in the dynamic integration of sensing into robot manipulation, a process that will hopefully make the robot exhibit skills that approach the human level.

While a combination of tactile, force, and position sensing carries the promise of enhancing the flexibility and robustness of robotic manipulation [6], the integration of different control strategies for multiple sensor modalities can become very sophisticated and unreliable at the present stage. From a minimalist point of view, one sensor modality should be preferred if it could yield sufficient information needed for executing a task.

*Support for this research was provided in part by Iowa State University, and in part by the National Science Foundation through a CAREER award IIS-0133681.

Meanwhile, industrial sensors are somewhat expensive for lab experiments, particularly those on small scales. A tactile array sensor could easily cost over $10,000. Less expensive force/torque sensors such as the ATI F/T-16 may be easily broken due to their narrow force and torque ranges.

In this paper we describe a low-cost 2-axis force/torque sensor capable of contact sensing and shape localization. Section 2 presents the sensor design, its underlying principles, and calibration. Section 3 introduces a strategy that implements the rolling motion of a jaw (mounted with the sensor) on an immobilized object. This strategy is used in the experiments in Section 4 for localizing the object relative to the jaw. Finally, Section 5 summarizes the work and outlines future improvements and directions.

1.1 Localization through Rolling

Our sensor design objective is to demonstrate a strategy that localizes a motionless curved object relative to a jaw rolling on its boundary. This strategy is illustrated in Figure 1. The

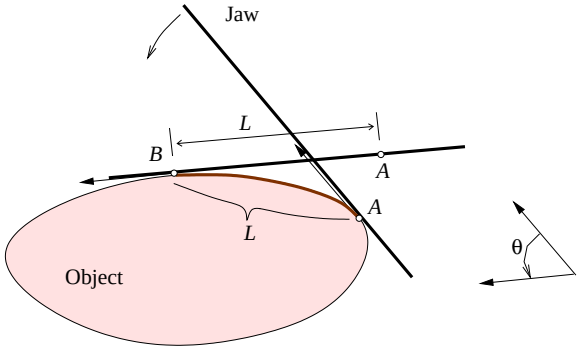

Figure 1: Localization of a rolling jaw on an object using the rotation angle θ and the distance L of contact movement.

location of contact is unknown on the object boundary. A touch sensor records the first contact location A on the jaw, which then rolls along the object boundary to complete a

rotation of θ (this is carried out by an Adept robot). Afterward, the new contact B is recorded.

In the mode of pure rolling, the distance L between A and B on the jaw equals the length of the boundary segment traced out by the contact. The rotation of the tangent as the contact moves through the segment, referred to as the *total curvature*, equals the jaw rotation θ, which is measured by the Adept controller. The problem of *object localization* now reduces to locating one or more curve segments with length L and total curvature θ on the boundary.

In the previous work [13], we gave an algorithm that guarantees to find (up to numerical resolution) all such segments in a running time on the same order as computing the object's perimeter through numerical integration. In case multiple segments are found, the algorithm examines the total curvatures of their following segments of some equal length.

Experimentally, we need to be able to locate contact on the jaw as well as generate (or approximate) the rolling motion. Simple force control will be needed. Thus a tactile array sensor is not preferred. Also a tactile array sensor would require direct contact with the object, likely complicating the jaw design. We have designed a simple 2-axis force/torque sensor to serve as a "wrist" which will be able to estimate contact after proper calibration.

1.2 Related Work

Salisbury [18] first proposed the concept of fingertip force sensing with a geometric approach for determining contact locations and orientations from force and moment measurements. This work was extended by Bicchi [2] who offered a mathematical solution to the problem of determining some global qualities of contact as well. Principles of contact position detection from force/torque measurements were also derived by Tsujimura and Yabuta [19] who went further to show how to detect various shapes. Brock and Chiu [3] designed a fingertip sensor consisting of four strain gauge half-bridges and used it to measure surface contact location and orientation as well as the center of mass. Zhou *et al.* [21] re-examined fingertip contact sensing with a focus on the elimination of gravitational biasing and error analysis, and demonstrated their sensor design with a hand manipulation system.

Contact forces and locations on a multi-link manipulator can be calculated from joint torque readings only. For the case of a multi-jointed link with an unknown object, Kaneko and Tanie [14] approximated the contact location between them as the intersection point of two postures of the link resulting from a small angular displacement under compliance. Grupen and Huber [10] used kinematic constraints and linear observers; they also calculated contact force from joint torque readings. Employing kinematics and nonlinear observers, Haidacher and Hirzinger [11] studied how multiple robotic fingers without tactile capability can utilize their relative velocities to estimate contact points and velocities on an object.

Measurements of contact may be considerably improved through integrating tactile information [9]. Fearing [7] designed a cylindrical tactile fingertip mounted on the Stanford/JPL hand for contact localization and regrasping. The fingertip was later employed [8] to determine principal curvatures on spheres, cylinders, etc. Based on continuum mechanics and photoelastic stress analysis, Cameron *et al.* [4] built a tactile sensor to detect changes in contact status and realize smooth phase transitions during a task. This idea of dynamic tactile sensing was extended by Howe and Cutkosky [12] to capture fine surface features during motion. Zhang and Chen [20] introduced two mappings from tactile images to contact states that can facilitate the feedback control.

Dynamic control of rolling contacts in the presence of tactile information has been studied in dexterous multi-arm manipulation [16], where nonlinear feedback schemes are employed. Rolling a manipulator on a fixed object generates compliant motion. Raibert and Craig [17] described a hybrid position/force strategy using an internal wrist sensor built on strain gauges to meet with manipulator trajectory constraints. Mason [15] synthesized control strategies for compliant motions by looking into the semantics of motion primitives.

Our sensor design is influenced by the work of Abe *et al.* [1] on implementing a 3-axis force/torque sensor sensitive to small reaction forces and torques in the plane but very stiff in other directions. We use a simple geometric strategy to generate the "effects of rolling", which are needed for localization.

2 Sensor Design

The main structure of the 2-axis force/torque sensor as shown in Figure 2(a) is an aluminum piece serving the purpose of a wrist that can bend along the inward/outward direction and twist about its axis of symmetry. Two chip sensors S_1 and S_2 from Bokam Engineering Inc. are glued to the wrist, one vertically and the other horizontally. Each chip sensor is a half-bridge design consisting of two strain gauges with electrical resistance of 900 ± 150 ohm. As shown in Figure 2(b), a rectangular plastic jaw (not drawn in scale) is attached to the bottom of the wrist.

Each chip sensor is wired to a set of electronics for conditioning and amplifying to yield an output in the range of 0–5 VDC. Let ΔV be the change of the voltage output of a chip sensor and ΔR the total change in the resistance R of its strain gauges. The *gauge factor* is a con-

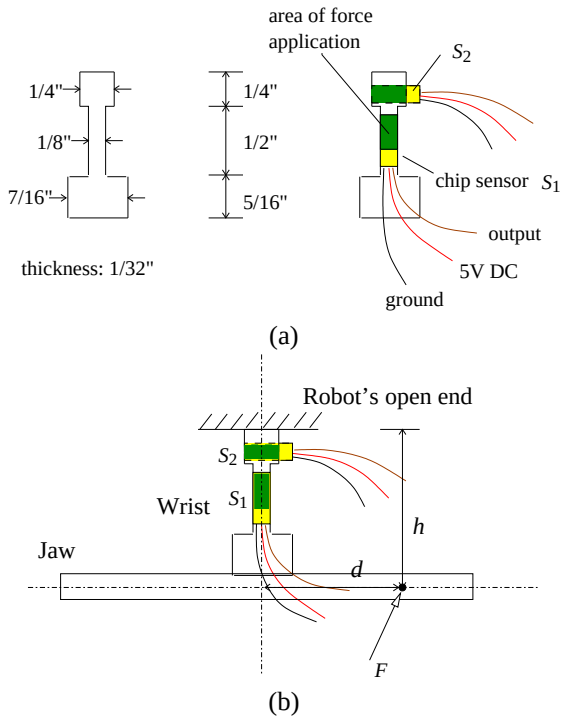

Figure 2: (a) A 2-axis force/torque sensor. Only the darkly shaded (or green) rectangular area at the tip of each chip sensor is sensitive to an applied force. (b) The force/torque sensor with a rectangular plastic jaw attached.

stant given as $GF = \frac{\Delta R/R}{\Delta L/L}$, where L is the normal length of a strain gauge and ΔL its variation. Ideally speaking, $\Delta L \sim \Delta R \sim \Delta V$, that is, ΔL is proportional to the change in the voltage readings of the chip sensor. Meanwhile, ΔL is also proportional to the stress and hence to the moment exerted on the material. So the voltage variation ΔV scales with the moment. Below we determine the ratio between the bending stress and the twisting stress and explain how it can be used for locating contact.

2.1 Stress Analysis

The chip sensor S_1 is sensitive to a bending moment about the horizontal axis of the jaw but not to a twisting moment about its vertical axis. The chip sensor S_2 is sensitive to a twisting moment but not to a bending moment. The coupling effects are assumed to be negligible in our analysis.

Figure 3 presents a top-down view of the two sections of the wrist on which the sensors S_1 and S_2 are mounted. In Figure 3(a), the stress at a point in the cross section in the y-z plane under a bending moment M_b is

$$\sigma_1 = -\frac{M_b y}{I_{zz}}, \tag{1}$$

where I_{zz} is the angular inertia of the cross section about

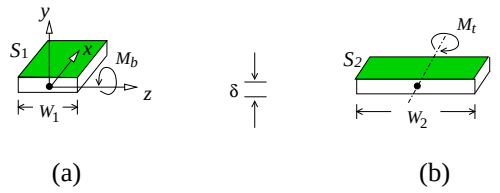

Figure 3: Two sections of the aluminum wrist where the chip sensors are mounted. In our design, $W_1 = 1/8''$, $W_2 = 1/4''$, and $\delta = 1/32''$. The widths match the length and width of the force application area on a chip sensor, respectively.

the z-axis [5, pp. 371-375]. We have that

$$I_{zz} = 2\int_0^{\frac{\delta}{2}} y^2 \cdot W_1 \, dy = \frac{\delta^3}{12} W_1. \tag{2}$$

Since the chip sensor S_1 is mounted at the boundary of the cross section, $y = \frac{\delta}{2}$. Substitute this and (2) into (1):

$$\sigma_1 = -\frac{M_b \cdot \delta/2}{W_1 \cdot \delta^3/12} = -\frac{6M_b}{W_1 \delta^2}. \tag{3}$$

So *the bending stress on S_1 is inverse proportional to the width of the cross section.*

The sensor S_2 detects a twisting moment M_t, as shown in Figure 3(b). Let σ_r be the stress at a point in the cross section at horizontal distance r from the center. Then we have

$$M_t = \int_{-\frac{W_2}{2}}^{\frac{W_2}{2}} |r| \cdot \sigma_r \cdot \delta \, dr = 2\int_0^{\frac{W_2}{2}} r\sigma_r \cdot \delta \, dr, \tag{4}$$

which has solution

$$\sigma_r = \frac{12M_t|r|}{W_2^3 \delta}. \tag{5}$$

Hence *the twisting stress is inverse proportional to the third power of the width of the cross section.* Since S_2 is glued on one edge of the cross section, the average twisting stress at all points inside S_2 is

$$\sigma_2 = \frac{12M_t \cdot (W_2/4)}{W_2^3 \delta} = \frac{3M_t}{W_2^2 \delta}. \tag{6}$$

In our design, we choose $W_2 = 2W_1 = 8\delta = 1/4''$. From (3) and (6) we obtain the ratio between the average twisting stress and the bending stress:

$$\frac{\sigma_2}{\sigma_1} = -\frac{M_t \delta W_1}{2M_b W_2^2} = -\frac{M_t}{32M_b}, \tag{7}$$

Suppose a contact force (of magnitude) F is applied normal to the jaw at distance d from its axis of symmetry and at distance h below the robot's open end (see Figure 2(b)).

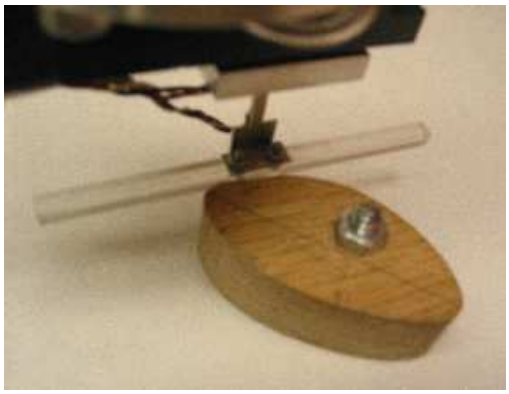

Figure 4: The setup for calibration (and localization later on).

Then $M_t = Fd$ and $M_b = Fh$. Substituting these two expressions into (7) yields

$$\frac{\sigma_2}{\sigma_1} = -\frac{d}{32h}. \tag{8}$$

In the ideal case, *the ratio between the stresses on S_2 and S_1, respectively, is a constant depending on d/h.*

The stress ratio should be proportional to the ratio between the variations Δv_2 and Δv_1 from the default readings on S_2 and S_1. In our task, the height h is maintained the same. Thus we can measure the horizontal location d of contact on the jaw from Δv_1 and Δv_2, after proper calibration.

Both chip sensors S_1 and S_2 have their default voltage outputs set around 2.5V by adjusting the potentiometers. Due to noise, the readings oscillate within ± 0.03V. To deal with noise, every output is averaged over three consecutive readings.

We have mounted the 2-axis sensor (along with the jaw) on an Adept Cobra 600 manipulator. To test the sensitivity of the wrist, we let the Adept command the jaw to move compliantly when touched. Continuous compliant motion of the jaw is generated while the touch is maintained. A touch in the middle results in pure translation of the jaw while a touch at a different location results in both translation and rotation.

2.2 Calibration

To calibrate the 2-axis sensor, the jaw in a fixed orientation repeatedly makes contact with an immobilized object as shown in Figure 4. Before making the next contact, the jaw translates by 1cm along the tangential direction. The contact point on the object boundary does not change but the contact points on the jaw as a result have 1cm spacings. During the contact, voltage readings of the sensor S_1 are maintained at some constant level (2.1V) when readings of the sensor S_2 are taken. This is achieved by simple feedback control under which the Adept manipulator translates the jaw over small distances along its normal direction while staying in touch with the object.

Figure 5 shows a cubic spline that interpolates eleven ratios between votage variations on the two chip sensors when the contact distance x from the wrist axis of symmetry varies from -5cm to 5cm with 1cm increments. Each ratio was an average over 90 pairs of readings by the chip sensors S_1 and S_2. The interpolating spline, referred to as the *calibration spline*, is relatively straight. Since v_2

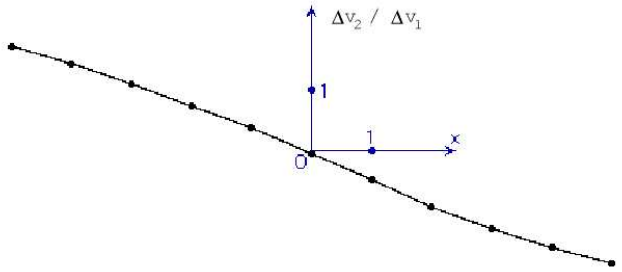

Figure 5: A cubic spline that interpolates the measurements in one calibration trial.

reflects the torque about the wrist's axis of symmetry, the spline agrees well with our theory that under constant contact force the moment scales with the contact distance from the axis. The discrepancy between the spline and a straight line could be attributed to various factors such as strain distribution over an area on the chip sensor not just at its center point, area contact (instead of point contact), nonlinearity of the voltage output, wire strain on the chip sensors, imperfect sensor mounting, possible tilting of the jaw, strain gauge noise, etc.

To determine the (horizontal) location of a contact on the jaw, we need only intersect the horizontal line of an average reading $\frac{\Delta v_2}{\Delta v_1}$ with the calibration spline. Measurement drifts due to time and temperature are relatively small. All the drifts tended to be in one direction.

We conducted tests on the accuracy of this spline-based calibration. In such a test, the jaw made contact at an arbitrary location on the object boundary. Then it translated at each step by a fixed distance along the tangential direction so that the contact point moved on the jaw in the opposite direction by the same distance. Meanwhile, the estimated movements from sensor readings using the calibration spline were then compared with the actual movements. The result of one such test is plotted in Figure 6.

3 Implementation of Rolling

As discussed earlier in Section 1.1, the rolling motion is a precondition for the localization algorithm to be applicable.

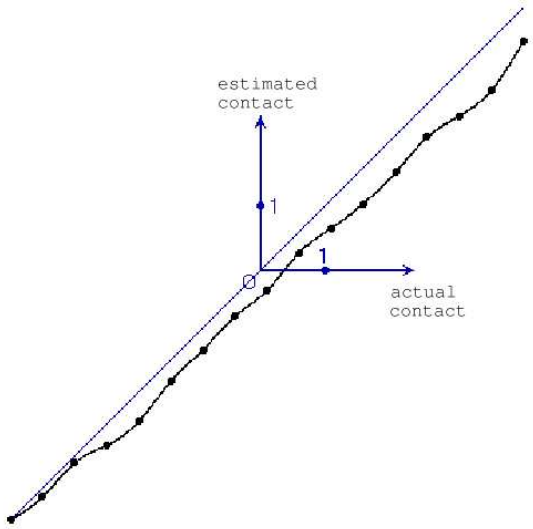

Figure 6: Calibration verification. The straight line segment interpolates 17 actual contact positions with a spacing of 0.5cm. The spline interpolates the corresponding sensor measurements.

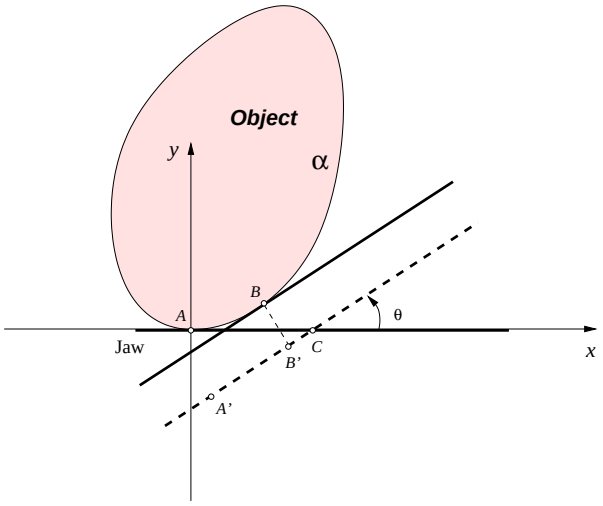

Figure 7: A rolling strategy. The jaw is initially at contact point A. It then rotates about the point C by a small angle θ. Finally, it translates along the normal direction to reestablish contact at point B.

Under rolling, the distance traced out by contact on the object's boundary can be measured as contact translation on the jaw. Here rolling is not realized through controlling joint torques by the Adept robot. Rather we adopt a simple strategy based on differential geometry as well as readings from the chip sensor S_1.

The jaw first establishes contact with the object so the readings from S_1 stay say, around 2.1V, which is slightly below the default value 2.5V. It then repeatedly carries out a sequence of rotations alternated with translations along the normal direction. More specifically, the jaw first rotates by a small angle. As it moves further "into" the object or away from it, the voltage reading of S_1 decreases or increases respectively. The jaw then backs up or moves forward in small steps accordingly until the readings return to around 2.1V.

Let us justify that the above strategy simulates rolling. We choose the origin to be at the contact location A before a rotation and let the x-axis be aligned with the jaw, as shown in Figure 7. There exists an arc-length parameterization $\boldsymbol{\alpha}(u)$ of the object boundary such that $\boldsymbol{\alpha}(0) = A$. The center of rotation on the jaw is at $C = (d, 0)$. Without loss of generality, we assume that $d > 0$. A counterclockwise rotation by an angle θ then breaks the contact. The initial contact point A on the jaw has been rotated to the position A'.

Next, the jaw translates along the normal direction to reestablish contact with the boundary curve at the point $B = \boldsymbol{\alpha}(s)$. The tangent of $\boldsymbol{\alpha}$ has rotated by θ as it moves from A to B. We have $\theta = \int_0^s \kappa \, du$, where κ is the curvature function.

Because $\boldsymbol{\alpha}$ is unit-speed, the contact moves a distance of s from A to B. The contact "movement" on the jaw is

$$\begin{aligned} |CA'| - |CB'| &= d + \left(\boldsymbol{\alpha}(s) - \begin{pmatrix} d \\ 0 \end{pmatrix}\right) \cdot \begin{pmatrix} \cos\theta \\ \sin\theta \end{pmatrix} \\ &= 2d\sin^2\frac{\theta}{2} + \boldsymbol{\alpha}(s) \cdot \begin{pmatrix} \cos\theta \\ \sin\theta \end{pmatrix}. \end{aligned}$$

Apply Taylor expansion at $s = 0$ to each of the terms on the right hand side of the last equation above and obtain

$$\begin{aligned} 2d\sin^2\frac{\theta}{2} &= O(s^2), \\ \boldsymbol{\alpha}(s) \cdot \begin{pmatrix} \cos\theta \\ \sin\theta \end{pmatrix} &= s + O(s^2). \end{aligned}$$

Derivation of the above uses the equations $d\theta/ds = \kappa$ and $\boldsymbol{\alpha}'(0) = (1, 0)^T$. So we have

$$|A'B'| = |CA'| - |CB'| = s + O(s^2).$$

When the rotation angle θ is very small, s is small. So *the distance $|A'B'|$ on the jaw approximates the length of the boundary segment from A to B.*

Figure 8 compares expected arc lengths and their estimates obtained during 23 rolling instances performed on an object at a known orientation. The rotation angle is kept at $\theta = 0.2$ degree in each instance. The jaw and the object were in contact almost all the time during the rolling. These rolling instances started at different points on the object boundary to avoid possible correlations between the results and the local geometry of one starting point. An expected contact movement was computed from the tangents

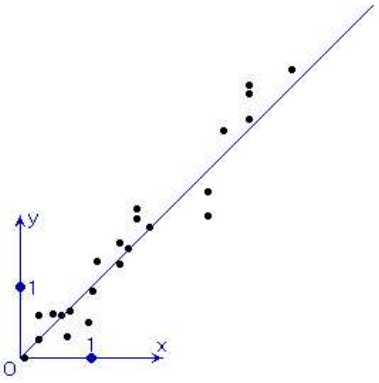

Figure 8: Comparisons between expected contact movements (x coordinates) and estimated contact movements (y coordinates) in 23 rolling instances. Each dot corresponds to the result of one such instance.

before and after the rolling based on the object's geometry. These tangents were determined from jaw orientations provided by the Adept controller. The contact movement estimates were provided by the force/torque sensor.

The executed motions were not pure rolling but rather their approximations. The estimation errors were higher in instances where the jaw passed high-curvatured portions of the object boundary. Discrepancies were likely also due to calibration inaccuracy, minor vibrations in the Adept controller, low contact friction between the plexiglass jaw and the wooden object, etc.

4 Experiments

Experiments for localization were conducted with flat wooden parts in cubic spline shapes. The experimental setup (with one part) is shown in Figure 4. Four instances of localization on two different parts are shown in Figure 9. In each instance, the jaw made the initial contact at some point a^* on the part boundary, rolled along the boundary for a while before stopping at another point b^*, then rolled again and finally stopped at a third point c^*. Though the boundary points a^*, b^*, and c^* were not known, their corresponding points on the jaw were estimated. The lengths of the two boundary segments from a^* to b^* and from b^* to c^*, denoted by $[a^*, b^*]$ and $[b^*, c^*]$, were thus estimated under the rolling assumption. Their total curvatures were the same as the corresponding jaw rotations read from the Adept.

In each instance, $[a_i, b_i]$ were all the boundary segments found by the localization algorithm from [13] that agreed with the length and total curvature estimates of the segment $[a^*, b^*]$. The ambiguities were then eliminated by examining the total curvatures of the following boundary segments

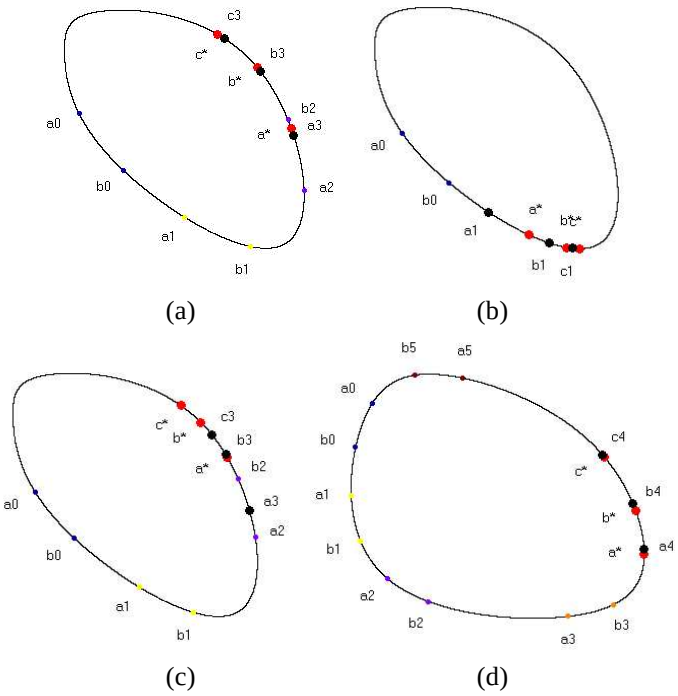

Figure 9: Localizing contacts on two objects with cubic spline shapes.

$[b_i, c_i]$ whose lengths were the same as the length estimate of $[b^*, c^*]$. The one with total curvature that best matched the Adept rotation was then chosen. The initial and final locations of the jaw on the object were then determined accordingly. They were a_3 and c_3 in the instances (a) and (c), a_1 and c_1 in (b), and a_4 and c_4 in (d).

The same part was used in the instances (a), (b), (c). In (a) and (d), the estimates were very close to the actual locations a^*, b^*, c^*. In (b), although estimates a_1 and b_1 had large errors, the estimate c_1 of the final location c^* was quite accurate. This is because curvature increases fast from a^* to c^*. Segments of the same total curvature starting quite apart from each other can end at points very close to c^*. This allows room for errors in estimating the length of $[a^*, c^*]$ by the force/torque sensor. On the other hand, if the curvature does not vary much from a^* to c^*, then estimation is not as robust to errors in the sensor, as in instance (c).

Total curvature estimates were simply the rotation angles of one of the Adept's joints and hence were very accurate. But length estimates were prone to errors in the force/torque sensor and the approximation of pure rolling. The success rate[1] of localization is currently around 45%.

[1] We considered localization a success if the located contact was "close enough" to the real one, as in the instances (a) and (d) in Figure 9.

5 Conclusion and Future Work

This paper describes an easily implementable 2-axis force/torque sensor capable of determining contact locations and useful for simple force control. Supported by an analysis from solid mechanics, the decoupling of strain gauge measurements simplifies sensor calibration such that no use of known load is necessary. This has eliminated one major source of calibration error. We have demonstrated that a special motion such as rolling on an object could be realized by a jaw mounted with the sensor, which meanwhile could localize itself on the object during the motion.

The force/torque sensor is implemented with very low cost (less than $300 excluding the 16-channel data acquisition board), making it desirable for lab experiments.

The accuracy of contact measurement needs further improvement. Localization should be made more active with contact sensing and rolling conducted simultaneously instead of one after the other. The jaw needs to be able to plan the rolling during an execution to improve the success rate (just like in a human touch).

The next step will be to demonstrate tasks such as grasping with two jaws, each equipped with a 2-axis force/torque sensor. We would also like to experiment with the sensor on constructing unknown 2-D and 3-D shapes through planned touch motions.

Acknowledgment The author is grateful to Joe Mesterhazy for writing a visual C++ driver for data acquisition and for implementing an interface between the Adept Cobra 600 and visual C++. He would also like to thank the following colleagues for generously sharing their expertise on force and tactile sensing: Ron Fearing, Ken Salisbury, Ralph Hollis, Greg Luecke, Richard Voyles, and Rob Howe.

References

[1] K. Abe, T. Miwa, and M. Uchiyama. Development of a 3-axis planar force/torque sensor for very small force/torque measurement. *JSME Intl. J., Series C: Mechanical Systems, Machine Elements & Manufacturing*, 42(1):376–382, 1999.

[2] A. Bicchi. Intrinsic contact sensing for soft fingers. In *Proc. of IEEE Intl. Conf. on Robot. and Automat.*, pp. 968–973, 1990.

[3] D. Brock and S. Chiu. Environment perception of an articulated robot hand using contact sensors. In *Robotics and Manufacturing*, pp. 89–96, 1978. PED-15.

[4] A. Cameron, R. Daniel, and H. Durrant-Whyte. Touch and motion. In *Proc. of IEEE Intl. Conf. on Robot. and Automat.*, pp. 1062–1067, 1988.

[5] S. H. Crandall, N. C. Dahl, and T. J. Lardner. *An Introduction to the Mechanics of Solids*. McGraw-Hill, Inc., 2nd edition, 1978.

[6] R. D. Howe *et al.* Grasping, manipulation, and control with tactile sensing. In *Proc. of IEEE Intl. Conf. on Robot. and Automat.*, pp. 1258–1263, 1990.

[7] R. S. Fearing. Some experiments with tactile sensing during grasping. In *Proc. of IEEE Intl. Conf. on Robot. and Automat.*, pp. 1637–1643, 1987.

[8] R. S. Fearing and T. O. Binford. Using a cylindrical tactile sensor for determining curvature. In *Proc. of IEEE Intl. Conf. on Robot. and Automat.*, pp. 765–771, 1988.

[9] S. J. Gordon and W. T. Townsend. Integration of tactile-force and joint-torque information in a whole-arm manipulator. In *Proc. of IEEE Intl. Conf. on Robot. and Automat.*, pp. 464–469, 1989.

[10] R. A. Grupen and M. Huber. 2-D contact detection and localization using proprioceptive information. In *Proc. of IEEE Intl. Conf. on Robot. and Automat.*, pp. 130–135, 1993.

[11] S. Haidacher and G. Hirzinger. Contact point identification in multi-fingered grasps exploiting kinematic constraints. In *Proc. of IEEE Intl. Conf. on Robot. and Automat.*, pp. 1597–1603, 2002.

[12] R. D. Howe and M. R. Cutkosky. Dynamic tactile sensing: Perception of fine surface features with stress rate sensing. *IEEE Trans. Robot. and Automat.*, 9(2):140–151, 1993.

[13] Y.-B. Jia. Localization on curved objects using tactile information. In *Proc. of IEEE/RSJ Intl. Conf. on Intell. Robots and Systems*, pp. 701–706, 2001.

[14] M. Kaneko and K. Tanie. Contact point detection for grasping an unknown object using self-posture changeability. *IEEE Trans. Robot. and Automat.*, 10(3):355–367, 1994.

[15] M. T. Mason. Compliance and force control for computer controlled manipulators. *IEEE Trans. Systems, Man, and Cybernetics*, SMC-11(6):418–432, 1981.

[16] E. Paljug, X. Yun, and V. Kumar. Control of rolling contacts in multi-arm manipulation. *IEEE Trans. Robot. and Automat.*, 10(4):441–452, 1994.

[17] M. H. Raibert and J. J. Craig. Hybrid position/force control of manipulators. *J. of Dynamic Systems, Measurement, and Control, Trans. ASME*, 102:126–133, 1981.

[18] K. Salisbury. Interpretation of contact geometries from force measurements. In M. Brady and R. Paul, ed., *Robotics Research*, pp. 565–577. The MIT Press, 1984.

[19] T. Tsujimura and T. Yabuta. Object detection by tactile sensing method employing force/torque information. *IEEE Trans. Robot. and Automat.*, 5(4):444–450, 1989.

[20] H. Zhang and N. N. Chen. Control of contact via tactile sensing. *IEEE Trans. Robot. and Automat.*, 16(5):482–495, 2000.

[21] X. Zhou, Q. Shi, and Z. Li. Contact localization using force/torque measurements. In *Proc. of IEEE Intl. Conf. on Robot. and Automat.*, pp. 1339–1344, 1996.